PERGAMON

International Journal of Multiphase Flow 25 (1999) 229–256

International Journal of Multiphase Flow

Single and double optical probes in air-water two-phase flows: real time signal processing and sensor performance

E. Barrau[a], N. Rivière[a], Ch. Poupot[b], A. Cartellier[a,*]

[a]*LEGI, Laboratoire des Écoulements Géophysiques et Industriels, UMR 5519, UJF-CNRS-INPG, BP 53, 38041, Grenoble cedex 9, France*

[b]*GICEP, ENSERG-INPG, BP 257, 38016, Grenoble cedex 1, France*

Received 12 December 1997; received in revised form 1 July 1998

Abstract

To progress in the understanding of phase detector capabilities, a first requirement has been fulfilled by manufacturing reproducible sensors. A second objective, investigated in this paper, is to diminish the sensitivity of the processing technique to the various criteria required to perform the signal analysis. A new real-time signal processing technique, based on optical probe responses during probe–interface interactions, is presented, and its objectiveness is demonstrated. When used with mono-fiber or dual-fiber sensors, it provides local void fraction and gas velocity measurements. The performance of these measuring chains is evaluated in various air–water two-phase flows for different probes. Possible mechanisms responsible for void fraction uncertainties are discussed. It is also shown that monofiber probes with a conical–cylindrical–conical extremity are well suited to measure gas velocities in dispersed two-phase flows. © 1999 Elsevier Science Ltd. All rights reserved.

Keywords: Optical probes; Monofiber probe; Double-probe; Gas–liquid flow; Phase detection; Gas velocity; Size distribution; Interfacial area density; Real-time signal processing; Measurement uncertainty

1. Introduction

Since the pioneering works of Neal and Bankoff (1963) and of Miller and Mitchie (1970), respectively, on resistivity and on optical sensors, phase-detection probes have become very common measuring devices for the investigation of gas–liquid two-phase flows. Apart from concentration measurements, the capabilities of single probes have been extended along various directions: current research concerns notably the determination of the size distribution (Liu

* Corresponding author.

0301-9322/99/$ - see front matter © 1999 Elsevier Science Ltd. All rights reserved.
PII: S0301-9322(98)00042-1

and Clark 1995), and the definition of flow regime indicators (Kozma 1995; Spindler and Hahne 1995). Meanwhile, bi or multiple probes have been extensively developed not only to measure gas velocity, but also to quantify the mean interfacial area density and the Sauter mean diameter (Revankar and Ishii 1992, 1993; Kataoka et al. 1994; Leung et al. 1995; Hibiki et al. 1997).

Despite these advances, phase-detection probes are not completely mastered. One basic problem is the evaluation of measurement uncertainties. A survey of the literature shows huge variations in probe performance (relative errors from −56 to +11% are reported for air/water or liquid/vapour freon (Cartellier and Achard 1991)). These could be attributed to the two-phase flow conditions considered and to the reference technique employed. More critical are the effects of probe design and signal processing. For the former, the latency length concept allows an objective comparison between probes (Cartellier 1990). In an idealised but interesting attempt, Carrica et al. (1995) related the void fraction error with the probe detection capability, or, more precisely, with the minimum detectable chord, which they evaluated as equal to the size of the probe extremity. Since this simplified model discards the complexity of the dewetting process, which is particularly clear at large impact angles (Cartellier and Barrau 1998a,b), it is unlikely that it can provide a reliable estimate of measurement uncertainties. Therefore, an experimental approach for the evaluation of sensor performance still appears unavoidable.

This argument is also strengthened by the fact that, regardless of the probe characteristics, the processing of raw signals required to locate the interfaces assumes a key role. Most existing processing techniques have been very clearly analysed by Zun et al. (1995). One can distinguish the "classical" techniques as based on absolute amplitude thresholding (single or double, on the signal or its slope), and these remain by far the most common (Schmitt et al. 1995; Garnier 1997; Hibiki et al. 1997). They share a common limitation that they exhibit a high sensitivity to the processing criteria (Cartellier and Archard 1991), essentially because they are incompatible with the actual response of probes interacting with interfaces. Taking into account such micro-scale phenomena has led to a new generation of procedures characterised by adaptative thresholding, i.e. thresholds evolving with the signal amplitude and shape. For example, van der Geld (cited by Zun et al. 1995) monitored the evolution of amplitude maxima, and distinguished full amplitude signals from the incomplete signatures usually associated with small chords: each population is processed with fixed but different thresholds. More refined procedures rely on a detailed analysis of every bubble signature: a wave-form analysis providing the amplitude and shape of each signal has been introduced by Cartellier (1992) while Zun et al. (1995), using the so called two-point discrimination, monitored the evolution of local extremum. Consequently, both criteria sensitivity (Cartellier 1992), and void fraction uncertainty (Zun et al. 1995) have been reduced compared with other techniques.

In this paper, the technique used by Cartellier (1992) is revisited with the aim of improving its objectivity by rationalising the detection criteria, and developing a real-time signal processing. Phase detection performances of the complete sensors are then quantified in air–water flows (Section 5).

The other question addressed in this paper concerns gas velocity measurements. The feasibility of such measurements using a monofiber probe has already been demonstrated (Cartellier 1992), but its reliability remains to be checked more systematically. This is

particularly true for the new probe geometries optimised for this purpose (Cartellier and Barrau 1998b). Hence, gas detection and gas velocity measurements have been combined in the same real-time processing, which is presented in Section 2. Some conical (named 1C) and conical + cylindrical + conical (named 3C) monofiber optical probes are qualified with regard to gas velocity in air–water flows in Section 5, where they are also compared with the widespread bi-probe technique.

2. Real-time signal processing for monofiber probes

2.1. Extraction of the characteristic function and of significant rise times

Starting from raw signals delivered by optical probes (Fig. 1), the identification of the gas dwell time is based on the determination of the dates of probe entry T_A and exit T_B through each bubble (Fig. 2). As shown by the analysis of the response of various probes (Cartellier 1990; Cartellier and Barrau 1998a,b), and discarding probe geometries delivering pre-signals, the very beginning of the signal rise corresponds to the detection of the disturbed interface location. Hence, to identify the bubble signatures, only two quantities have to be evaluated: the amplitude corresponding to a fully wetted probe V_L and the peak to peak noise amplitude V_B. Since discrimination is not possible within the noise, the presence of a bubble is detected

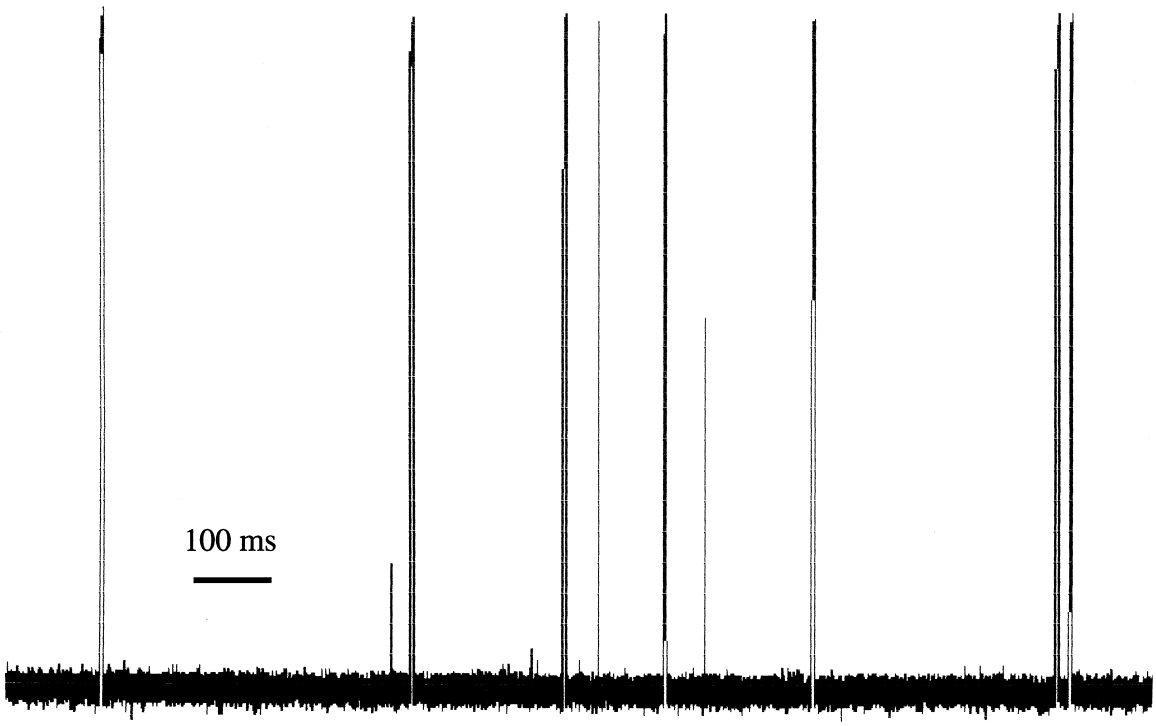

Fig. 1. Actual bubble signatures from a conical optical fiber (sampling frequency 20 kHz, $\Delta V \approx 4$ V).

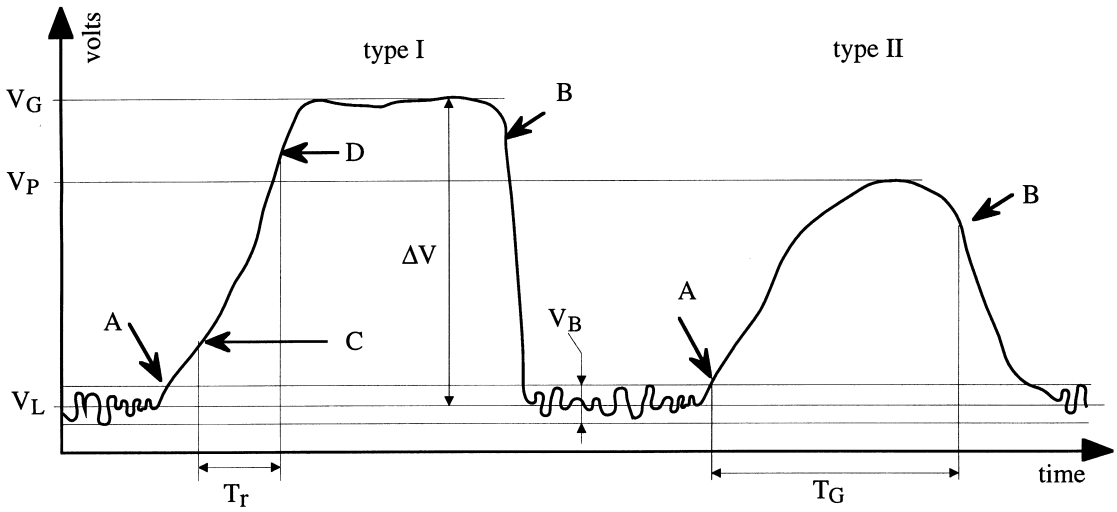

Fig. 2. Sketch of characteristic events detected on bubble signatures.

whenever the signal exceeds the level $V_T = V_L + CS1\ V_B$, where CS1 is a security coefficient accounting for the randomness of the noise. For a gaussian noise, the coefficient $CS1$, which varies between 0.5 and 1, is typically set to 0.75, so that the probability of interpreting a noise peak as a bubble is less than 0.005. Note also that since bubble signatures lower than level V_T are ignored, it is recommended to ensure a good enough signal to noise ratio (SNR) to minimise V_T. The actual entry date T_A is determined by the occurrence of a signal anterior to the beginning of the event detected, and whose amplitude exceeds the base level V_L by an amount of $V_B/2$. Hence, T_A is determined by the parameters V_L and V_B; its dependency on $CS1$ being only conditional, the above procedure differs from absolute thresholding.

For the exit date T_B, an analysis of the shape of the signature is first required. If a plateau exists, the de-wetting process has been almost completed (neglecting here the influence of tiny droplets stuck on the fiber), and the ensuing wetting process produces a steep signal decrease as shown by the type I signature in Fig. 2. Denoting V_G the mean plateau level, the exit date T_B corresponds to an amplitude $V_G - CS3\ (V_G - V_L)$, where according to the water entry responses observed in well-controlled conditions (Cartellier 1990, Cartellier and Barrau 1998a,b), $CS3$ ranges from a few percent up to 30%. The situation is less clear for low amplitude, usually bell-shaped, signatures, such as the type II signal in Fig. 2, which is characteristic of incomplete probe drying. It has been decided to apply again the above criteria, replacing V_G by the peak amplitude V_P. To finely adjust the parameter $CS3$ in this case, more work is needed to locate the rear interface on type II signatures. At present, values in the range of 5–20% for $CS3$ are currently used, the default value being 10%. In all cases, V_G or V_P being computed for each event, $CS3$ is the only free (but strongly bounded) parameter intervening in the detection of T_B.

The wave-form analysis is based on a sub-sampling controlled by a single amplitude parameter WA. Starting from the event T_A, sample points are tagged whenever the amplitude difference with the previous tagged point is at least WA. This sub-set of tagged events

reproduces the shape of the waveform with a low number of data. A compromise must be sought between a refined enough tagging leading to acceptable uncertainties on V_G or V_P, and a reduced number of computations to ensure real-time detection by the processor. To estimate this optimum, tests have been performed on actual signals collected in bubbly flows and combined with random Gaussian noise. The first wave-form considered corresponds to a type I signature, while the second one is of type II. Defining ΔV as the maximum amplitude difference observed for a wet and a dry probe, the following constraints were obtained:

- For $WA/\Delta V < 0.25$, the relative uncertainty on the gas dwell time $T_G = T_B - T_A$ mainly due to variations in the location of T_B, is zero for type I and less than $\pm 1\%$ for type II signatures.
- For $WA/V_B > 0.75$, the plateau detection is 99% successful, and the amplitude V_G is estimated within $\pm 1\%$ for the signal-to-noise ratio (SNR = $\Delta V/V_B$) considered (from 5–20).

Moreover, to render the CPU time compatible with the sampling frequency and the bubble arrival rate, $WA/\Delta V$ must not be too small. The precise limit depends on the capabilities of the CPU and on the nature of the flow. Typically, for the system described in Section 2.2, $WA/\Delta V$ was not less than about 0.1:0.1 is the default value.

Once the above information is at hand, it is straightforward to measure the rise time T_r. This duration T_r is determined from two characteristic points C and D located on the signal rise and corresponding, respectively, to a lower and an upper threshold (Fig. 2). Threshold values, defined as a percentage of ΔV, must correspond to those used during probe calibration. Also, since rise time/velocity correlations are essentially valid for close to normal impacts (Cartellier and Barrau 1998b), meaningful transitions must be selected among the signatures. For 2 mm bubbles, it has been found that complete de-wetting is ensured when the plateau duration exceeds the rise time. This corresponds to incidence angles less than about 40°, for which the rise time/velocity correlation is accurate within 10% for 3C probes. Similar behaviour is expected to hold for bubbles in the whole range of ellipsoidal and rocking regimes, i.e. roughly for $E\ddot{o} = Gd^2/\sigma < 40$ (Clift et al. 1978) where G is the pressure gradient, d the bubble size, and σ the surface tension. Therefore, in addition to the presence of a plateau, the selection relies on the criteria $T_G/T_r > CS2$, where the coefficient $CS2$ must not be less than unity. For the selected transitions, T_r is computed as the difference $T_D - T_C$.[1]

The real time procedure furnishes for each signature the dates T_A and T_B (referenced from the beginning of measurements), the amplitude V_G or V_P, the rise time T_r, when applicable, and a code specifying the nature of each waveform according to the validated criteria. It is worth underlining that this procedure is valid while the signal amplitude at the liquid level remains stable during the entire measuring duration. Departure from this situation was never observed in air–water flows except in the presence of strong accidental fouling. For liquid–liquid systems in which one phase sticks preferentially to the probe, and for mist flows, adaptation of the above criteria is required.

[1] To account for variations of the plateau amplitude observed notably in viscous liquids, a condition $V_G \geq V_R$ has to be added where the reference level V_R remains to be evaluated. In air–water two-phase flows, the plateau amplitudes are fairly stable and this criterion is not required.

Slope thresholding (as described in Cartellier 1992) has not been implemented in the real-time procedure for two reasons. First, the large variations of the rise time with impact angle indicate that absolute slope thresholding is inappropriate. Second, differentiation of the signal requires some amount of filtering and/or splining which drastically diminish the performance of real-time processing.

2.2. Architecture and post-processing

To account for the finite response time of the optodetector (typically 1 μs) and to reduce the noise, the raw signal is usually low-pass filtered (Butterworth filter, 24 dB/octave) before digitalisation. The sampling frequency of the A/D converter (10 bits) can be adjusted up to a value of 1 MHz. The data are then processed by a digital signal processor DSP 56001 (fixed mantissa) driven by a 20 MHz clock, with a resulting computation power of 10 Mips. The information T_A, T_B, V_G or V_P and eventually T_r, are stored in SRAM (128 Kwords, 24 bits) and the absolute dating of these events is ensured by an external clock up to a duration of 4 h. To check the convergence, these data are also transferred to a personal computer through a FIFO memory, for ploting the time evolution of the gas dwell-time and rise-time distributions as well as the void fraction.

The real-time performance of this system has been evaluated using periodic identical trapezoidal wave-forms (with *WA* set at its default value). Rise-time detection was first excluded. For a given sampling frequency, the curves of Fig. 3(a) define the regions where no event is missed as a function of the wave-form (or "bubble") arrival frequency and the "apparent void fraction". For example, at a digitalisation rate of 500 kHz, and for a "bubble" arrival frequency of 10 kHz, the maximum void fraction is about 25%. These performances are not fully representative of what may happen in real flows, notably because the arrival frequency can evolve with time, leading to a saturation of the processing capacity of the DSP. Let us nevertheless mention that void fraction measurements have been achieved without any loss of information at a digitalisation rate of 500 kHz, for a bubble arrival frequency of 8 kHz and a void fraction of about 10% (Fauquet 1995). In a second series of tests, rise time measurement was included (T_r was set to 10 μs for all tests) and the corresponding performance is given in Fig. 3(b), where the curves correspond to the detection and the analysis of all events. As expected, for a given bubble arrival frequency, the maximum apparent void fraction is reduced. Also, these limits are more sensitive to the bubble arrival frequency than those obtained for void detection alone.

Post-treatment by a personal computer provides a variety of information (Cartellier 1999). In this paper, we will be interested only in the local void fraction ε and the gas velocity. ε is given classically by the sum of all gas dwell times detected divided by the duration of the signal which has been scrutinised. The velocity U of a gas inclusion is obtained by inverting the correlation T_r (U) which has to be determined for the probe and the fluids considered, using either a separate experiment or from the probe geometry (Cartellier and Barrau 1998a,b). A mean gas velocity can be computed as the arithmetic average of all U values. However, this estimate is biased, since U is available only for a subset of all bubbles detected. To correct this bias, at least in part, a velocity U^* is evaluated for all gas inclusions using a time interpolation between the nearest values for U. Beside, assuming that the velocity in the gas inclusion and

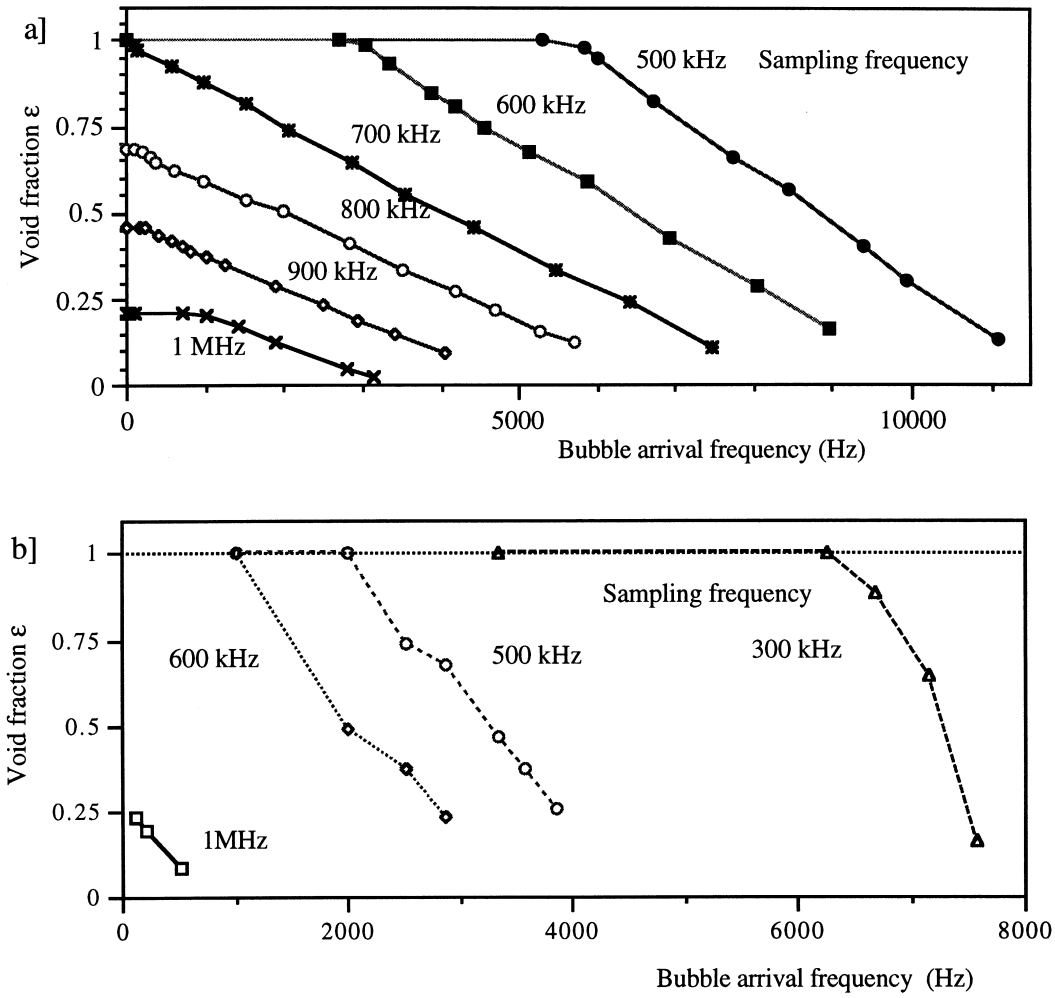

Fig. 3. Real-time capabilities using generated periodic trapezoidal waveforms: (a)T_A, T_B, V_G, V_P detection; and (b) T_A, T_B, T_C, T_D, V_G, V_P detection.

along the chord bisected by the probe equals the velocity U, a phase averaged velocity U_G can be determined according to:

$$U_G = \sum_{j=1}^{N} T_{Gj}\, U*_j \Big/ \sum_{j=1}^{N} T_{Gj} = \sum_{j=1}^{N} T_{Gj}\, U*_j /(\varepsilon\, T) = \sum_{j=1}^{N} C_j/(\varepsilon\, T), \tag{1}$$

where N denotes the total number of bubbles detected during the measurement duration T. The last equality in (1) introduces the chords C_j intersected by the probe. The local gas volumetric flux j_G equals εU_G. Note that the interpolation mentioned above is expected to be valid when the proportion of signatures with a rise time detection is large, and when these measurements are rather uniformly distributed in time.

2.3. Sensitivity analysis for void fraction measurements

Although recommendations have been given in Section 2.1 for the coefficients involved in the processing, their actual influence on the measurements must be quantified. For this purpose, a conical probe has been immersed in a bubbly flow at a fixed position, and flow conditions have been held constant. Measurements over a 300 s interval have been repeated for various sets of the coefficients *CS*1, *CS*3 and *WA*, including values outside the recommended ranges. The results in terms of void fraction and mean gas dwell time are given in Fig. 4: the relative deviation is less than $\pm 2\%$ for both measured quantities. This is also the magnitude of the reproducibility as shown in Fig. 4(d), where five runs obtained for the same coefficients are plotted: the void fraction evolves within $\pm 2.4\%$ while the mean gas dwell time relative variation is $\pm 1.7\%$. Since the sensitivity of phase detection has the magnitude of the reproducibility, it can be concluded that the proposed processing is a fairly objective tool. The large SNR ensured during these tests (about 80) has allowed testing *CS*1 and *WA* far above their recommended range, illustrating thus, the response of the processing. For lower SNR, the constraints delineated in Section 2.1 must be strictly fulfilled to avoid erroneous measurements.

A second aspect deserves attention. Indeed, the quantification of V_L and V_B are crucial for the signal processing, and an automatic detection of these amplitudes has been implemented in the system. However, particularly at high void fractions, this detection could be unsuccessful and the determination of V_L and V_B must be done by the operator. It is thus worthwhile to evaluate the accuracy required on these parameters. The influence of V_B being the same as *CS*1, let us concentrate on the parameter V_L. Let us fix the values V_{L0} and V_{B0} declared to the system, so that the threshold V_T is constant and equals $V_{L0} + CS1\ V_{B0}$, and let us vary the actual liquid level V_L of the raw signal. The detection of bubble signatures evolves as sketched

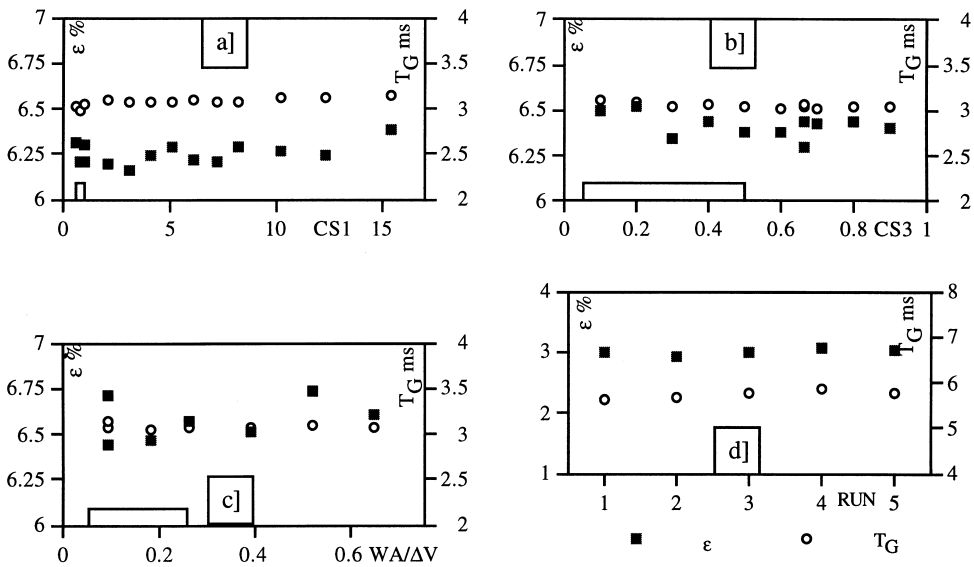

Fig. 4. Sensitivity to *CS*1, *CS*3, *WA* and reproducibility (closed boxes define the recommended ranges of variation).

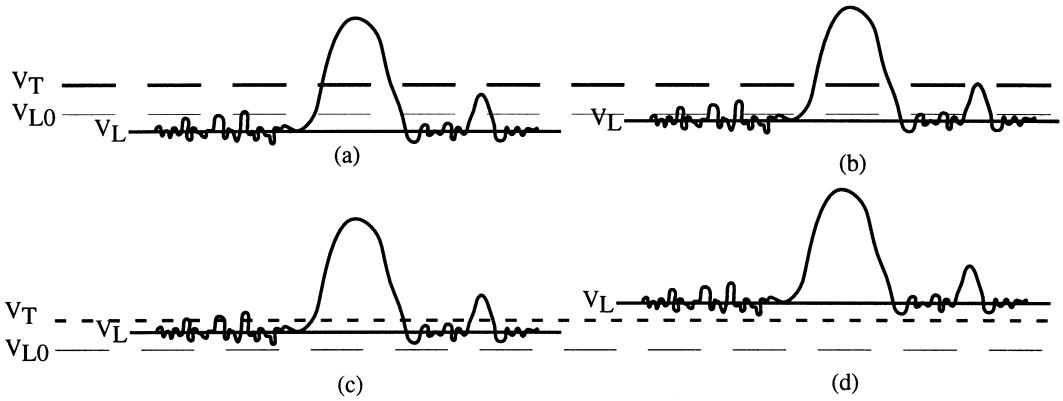

Fig. 5. Sketch of the evolution of the detection with the actual liquid amplitude for a fixed threshold level.

in Fig. 5. For V_L much lower than V_T, low amplitude signatures are missed, Fig. 5(a). Note that, contrary to absolute thresholding techniques, the gas dwell times of the large-amplitude signatures are still correctly determined, thanks to the condition imposed for the detection of the entry dates. Low-amplitude signals become more accurately processed as V_L increases, until V_L reaches V_{L0}, which corresponds to nominal operation, Fig. 5(b). As V_L is increased further, some noise peaks are interpreted as bubbles. Such erroneous detections become more numerous as V_L increases and the void fraction grows drastically while small gas dwell-times overwhelm the distribution of T_G, Fig. 5(c). This situation is maintained while a thresholding is possible, that is roughly until $V_L \approx V_T + V_{B0}/2$. For higher V_L amplitude, the system no longer detects any event, since no thresholding occurs, Fig. 5(d). All these trends have been confirmed experimentally, as shown by the evolution of the void fraction and the mean gas dwell-time with the ratio V_L/V_{L0} (Fig. 6). Notably, for this ratio in the range [0.75, 1], the relative variations of the measurements are within $\pm 1\%$, and no detection occurs for a ratio above 1.2. It can be concluded that the accuracy required on the measurement of the liquid level V_L must be not less than half the peak-to-peak noise amplitude V_B: this is not a very stringent

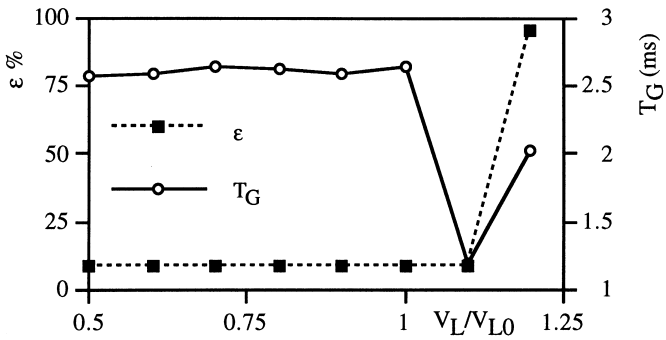

Fig. 6. Evolution of void fraction and mean gas dwell-time with the actual liquid amplitude.

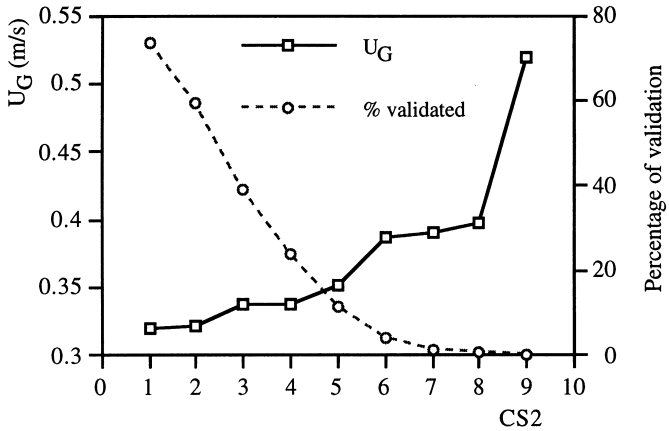

Fig. 7. Evolutions of the mean gas velocity and the percentage of rise time measurements with the selection criteria *CS*2 for a 3c probe in a bubbly flow.

requirement. The same recommendation must be followed with regard to the stability of the liquid level during data collection.

2.4. Sensitivity analysis for velocity measurements

From the rise-time definition, it is clear that the liquid level V_L and the amplitude of the plateau V_G must be accurately determined. While V_L is calibrated before measurements, V_G is a computed quantity. As shown in Section 2.1, its determination relies mainly on *WA*, and constraints have been defined to ensure a good accuracy on the estimate of the plateau amplitude. Thus, the only parameter not yet considered is the coefficient *CS*2, which has been introduced to select meaningful signatures. When *CS*2 is increased, velocity measurements are only performed on the largest bubbles present in the flow, inducing a bias in the statistics. On the other hand, *CS*2 below unity means that the correlation $T_r(U)$, established so far for normal impacts, is unduly applied to all kinds of probe–interface interactions. A typical evolution of the mean gas velocity U_G with *CS*2 is given in Fig. 7. These data have been collected with a 3C probe in an air–water dispersed flow at a void fraction about 2.4%. As expected, the mean gas velocity U_G increases steadily with *CS*2, but, for *CS*2 in the range [1, 5], the evolution is limited to 9%. Note that measurements performed for *CS*2 higher than 5 are less significant, since the percentage of validated signals becomes less than 10%. According to these trends, the default value for *CS*2 is set to 2. During post-processing, it is always possible to strengthen the selection by introducing higher values for *CS*2.

3. Real-time signal processing for bi-probes

As mentioned in the introduction, it is worthwhile comparing the velocity measurement performed with single probes to the classical technique, based on two sensitive tips placed some

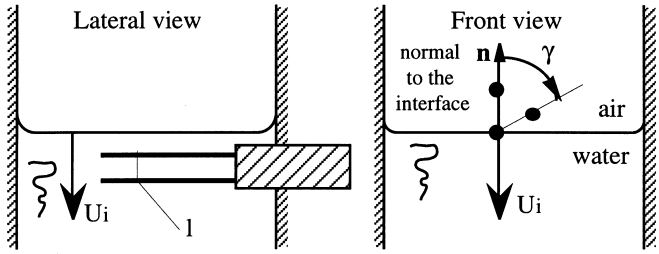

Fig. 8. Experimental set-up for the analysis of the response of double-probe on a well-controlled interface.

distance apart. No geometry optimisation has been performed on bi-probes. The sensors used are composed of two parallel fibers, whose axes are perpendicular to the main flow direction. The distance l between their tips, of the order of 1 mm, is less than the size of the bubbles present in our experiments.

3.1. Tests on controlled interfaces

The response of a commercially available double-probe composed of stretched silica fibers (core diameter 100 μm, external diameter 140 μm), has been analysed on well-controlled plane interfaces obtained by emptying a vertical duct, as sketched in Fig. 8. The distance l equals 1.08 mm $\pm$ 2%, the length of the fibers outside the casing tube (3 mm outer diameter) is about 12 mm. The interface velocity U_i and the angle γ between the normal to the interface and the line joining the two tips, have been varied. The interface velocity is known with a $\pm$1% accuracy, and the angle γ is determined within a few degrees. The error on the measured velocity is quantified by $(1 \cos \gamma/\Delta T - U_i)/U_i$, where ΔT is the measured transit time.

Two definitions of ΔT have been tested. ΔT has been evaluated from the entry dates $T_{A1} - T_{A2}$, and from $T_{D1} - T_{D2}$ i.e. the time lag between the characteristic points D located at a threshold of 90% of ΔV (the subscripts 1 and 2 are used to identify each optical fiber). According to the error in velocity plotted in Fig. 9 for $\gamma = 0°$, velocities are strongly overestimated when defining ΔT as $T_{D1} - T_{D2}$. Therefore, the entry date method should be preferred.

The effect of the orientation γ has also been investigated for a transit time defined by the entry dates. Error distributions for velocities ranging from 1 cm/s to 3 m/s are given in Fig. 10. For $\gamma = 0°$, the error is roughly symmetrically distributed between over- and underestimates with a magnitude of about $\pm$15%, which is in agreement with the observations of Rossi (1996) on small bubbles. However, as γ increases, the error distribution is strongly shifted towards an underestimation of the interface velocity. This is, again, a consequence of disturbances induced by the probes.[2]

The strong uncertainties observed at large inclinations are probably not fully representative of what occurs in actual two-phase flows, because of the special configurations considered here

[2] Let us also mention that additional tests have shown that the velocity becomes systematically overestimated above about 4–5 m/s due to the bending of the fibers, which reduces the actual distance between tips.

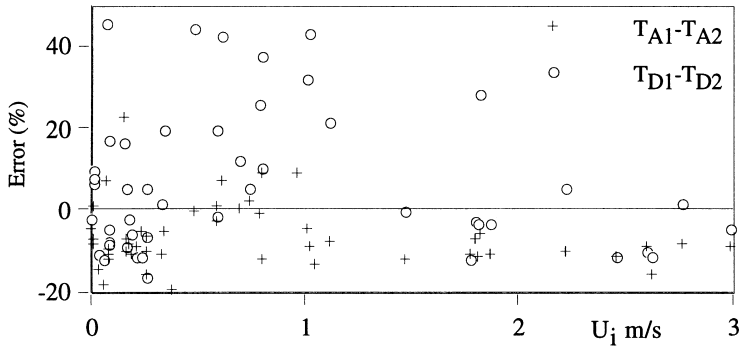

Fig. 9. Error in interface velocity (at $\gamma = 0°$) for two definitions of the transit time ΔT.

concerning both the probe and the interface. However limited in their scope, these tests have underlined the crucial effect of interface deformation on the response of bi-probes, indicating that although the double probe technique is considered as classical, a more detailed understanding of its drawbacks are required before these sensors can be considered as a reference tool. Note that the above observations are expected to change when using a bi-probe facing the main flow.

3.2. Processing criteria and sensitivity

Since we are interested in the statistics of the gas velocity, a time analysis is required instead of a cross-correlation of the two signals. Signal pairs must be identified to define the transit times of interfaces, and it is well known that errors occur from bubbles not intercepted by both sensors. There is no definite agreement about the criteria needed to discriminate these non-associated signals. The most usual test consists of setting a maximum relative differences between the gas dwell-times T_{G1} and T_{G2} detected by each sensor. For example, the parameter

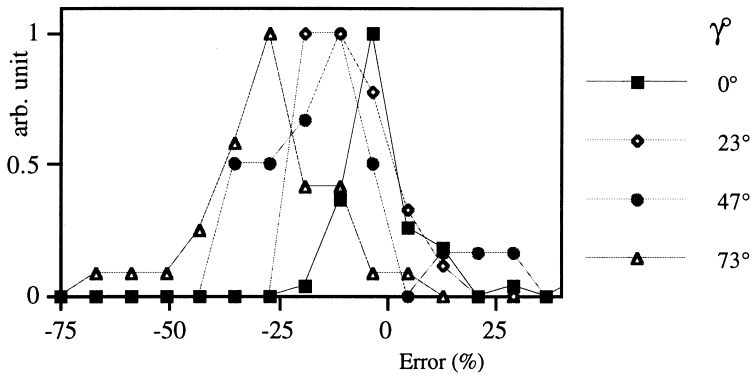

Fig. 10. Distribution of the error in interface velocity measurement using a bi-probe for various orientations γ with respect to a plane interface.

$CSP = |T_{G1} - T_{G2}|/T_{G1}$ is set to less than 30% by Leung et al. (1995). This kind of criteria has been retained in our processing. Also, a maximum waiting time is sometimes imposed. Here, the search for a companion signal on the second channel is stopped when a new signal occurs on the first probe.

The system for processing double-probe signals is based on the architecture described in Section 2.2. Since a single A/D converter digitizes the two signals, the maximum sampling frequency is reduced to 500 kHz. The phase-detection procedure presented in Section 2.1 is applied in real-time to each channel, so that the succession of the characteristic dates T_{A1}, T_{B1} and T_{A2}, T_{B2} are determined with the same time encoding. A default value $CSP = 5\%$ is used for a real-time plot of the transit times. The post-processing is similar to that presented in Section 2.2 for monofiber probes, except that the pairing of signatures can be performed for any value of the coefficient *CSP*. This feature has allowed to check the sensitivity of velocity to *CSP* on the same signals. This test has been performed in a bubbly flow, with a local void fraction of about 4%. The scanning time was 300 s, during which more than 4000 bubbles were detected. The void fraction detected by the downstream probe was 4% lower than that detected by the upstream sensor, mainly due to a decrease in the average bubble arrival frequency. As shown in Fig. 11, the average gas velocity is weakly dependent on the pairing parameter *CSP*, provided that its value is at least 5%. The fact that this trend holds up to high values of *CSP*, is due to the specific conditions of this experiment, namely a low void fraction and bubble sizes in the range 2–5 mm. A much higher sensitivity is expected for larger void fractions and/or wider size distributions. The percentage of pairing is also plotted in Fig. 11: as expected, it increases steeply as the pairing criteria is relaxed. It should be mentioned that this validation rate must be not less than say 20% to ensure a meaningful interpolation of velocities. This corresponds to a coefficient *CSP* of at least 5%, and 5% has been used for the qualifications.

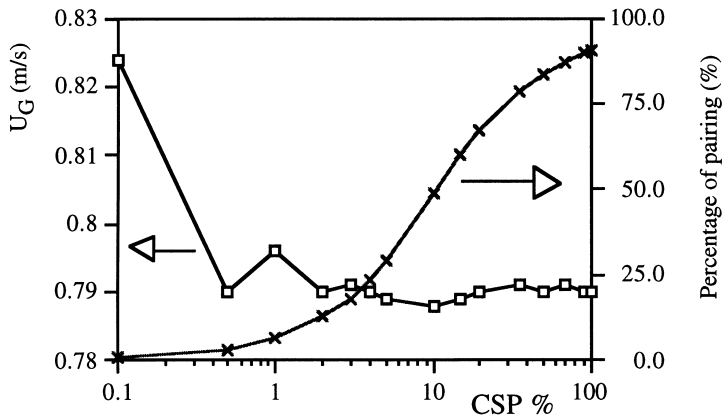

Fig. 11. Evolution of the gas velocity and the percentage of pairing with the pairing criteria for a bi-probe in a bubbly flow.

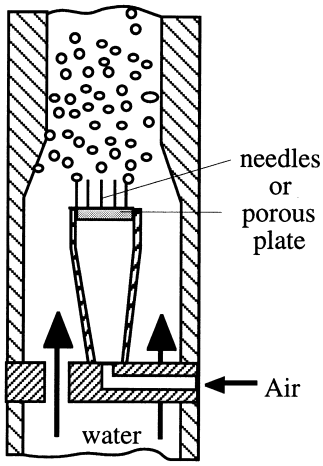

Fig. 12. Gas injection device.

4. Experimental set-up and procedure

4.1. Test facility and global measurements

To qualify the performance of various optical probes associated with the real-time processing presented above, profiles of local measurements are integrated and compared with global quantities, namely the volumetric gas flow rate Q_G and the volumetric gas fraction R_{G3}. For this purpose, co-current, upward two-phase flows in a vertical duct have been considered. The plexiglass duct, with a $D = 50$ mm internal diameter, is 5 m long. Clean and dry air is injected at the bottom of the duct (Fig. 12). Three types of injectors were used: a porous plate, and 2 cm long capillaries with an internal diameter of either 90 or 200 μm. In the dispersed regime, bubble sizes range from 2 to 6 mm. Three volumetric water flow-rates Q_L were considered, corresponding to liquid superficial velocities $J_L = Q_L/(\pi D^2/4)$ of 0, 0.2 and 1 m/s. The volumetric gas flow-rate Q_G was measured with a battery of calibrated flow meters with an accuracy not less $\pm 2.5\%$. Q_G (evaluated in the test section) has been varied from 3 to 3830 Nm^3/h. The flow regime ranges from bubbly to slug flow.

To measure the volumetric gas fraction R_{G3}, two ball valves, positioned 2 and 4.5 m downstream from the injection, can be closed simultaneously using a mechanical link: the closure time is 0.1 s. R_{G3} is deduced from the volume of water trapped between the valves with an uncertainty of 0.5% of void. For each flow condition, these measurements were repeated five times with a reproducibility of 0.2% of void in the dispersed phase regime[3] and 2% for slug flow. The larger variance for slug flows is due to the random trapping of slugs. For steady state and "fully developed" conditions, the cross-sectional area average gas fraction R_{G2}

[3] In a previous paper (Cartellier et al. 1996), huge uncertainties on R_{G3} (up to 25%) at gas fractions less than 5% were reported. This defect which was due to a modification in the aperture of the main liquid valve when activating quick closing valves, has been corrected. The 0.5% uncertainty of R_{G3} holds now for the whole dispersed regime.

should equal the volumetric gas fraction R_{G3}. Although the two-phase flow develops between the two ball valves, the axial change in R_{G2} is expected to be less than 1% void, according to the data obtained by Grossetête (1995) in conditions close to ours.

4.2. Local measurements

Various probes have been used during the qualifications. Some of their characteristics, including the geometry of holding tubes and their orientation with respect to the main flow direction are reported in Table 1. The stretched probe is a product from Photonetics company, while the others including conical and conical–cylindrical–conical probes are homemade. The double-probe used during the qualifications is composed of two conical probes.

The measuring section is located midway between the quick-closing valves. In this section, optical probes are translated along a diameter, and their position is measured with a comparator (uncertainty ± 0.5 mm). The two quantities evaluated are the area gas fraction R_{G2} defined by:

$$R_{G2} = \int_0^{2\pi} \mathrm{d}\theta \int_0^{D/2} \varepsilon(\theta, r)\, r\, \mathrm{d}r/(\pi D^2/4), \tag{2}$$

and the measured gas flow rate Q_m given by:

$$Q_m = \int_0^{2\pi} \mathrm{d}\theta \int_0^{D/2} j_G(\theta, r)\, r\, \mathrm{d}r, \tag{3}$$

where r denotes the distance to the duct axis and θ the polar angle.

Table 1
Characteristics of the probes used during the tests

Probe	Conical	Stretched fiber	Cone+cylinder+cone	Double-probe (conical tips)
Orientation	Parallel	Perpendicular	Perpendicular	Parallel
Holding tube	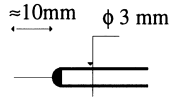	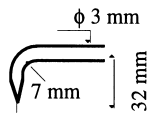	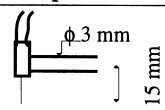	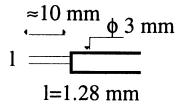
Sensitive tip	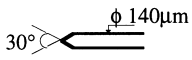	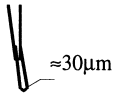	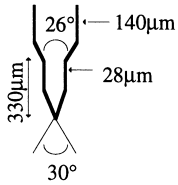	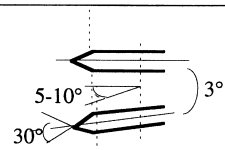
Spatial range accessible (mm)	-25 ; +25	-22.6 ; 23.4	-24.7 ; +22	-25 ; +25

Sets of about 30 probe positions were considered for each flow condition. The measuring time was 5 min for each location. Note that the processing criteria were set to their default values and held constant. The sampling frequency has been chosen according to the probe and the flow conditions. When performing rise-time measurements, sampling frequencies were typically 100 kHz for the 3C probe and 600 kHz for the stretched probe. Note that all the conditions considered are well within the real-time capabilities of the system presented in Fig. 3(a) and (b). The integrations involved in (2) and (3) were performed using linear, cubic or spline interpolations between the measured discrete values. No significant differences were noticed between these techniques. Measurements at the wall are possible only for the conical and double tip (Table 1); in all other cases, the conditions $\varepsilon = 0$ and $U_G = 0$ have been imposed at walls.

As shown by the examples provided in Fig. 13, the profiles were never totally axisymmetric. This is partly due to disturbances induced by the holding tube, which results in slightly higher void fractions on the right-hand side of the profiles, i.e. in the zone opposite to the wall supporting the probe. To account for this asymmetry, two integrals were performed by extending left (from $-D/2$ to 0) and right (from 0 to D/2) profiles over a 2π angle. The arithmetic average of these two quantities is considered as the measured value: the algebraic error is then defined as the measured value minus the reference value, divided by the reference value. The "left" and "right" integrals are used to define uncertainty bars on all the plots presented in the next section with larger bars corresponding to greater profile asymmetry.

5. Optical probe performance

5.1. Error in void fraction measurements

The relative error on the gas fraction is given in Figs. 14–16 for various probes. For the flow conditions defined by the intervals $R_{G3} \in [0.01, 0.27]$ and $J_L \in [0, 1]$ in m/s, the error evolves between −0.8 and −16%. Some general comments can be made about the data:

- The relative error on the void fraction is only marginally sensitive to the probe orientation. Such behaviour has been also observed by Zun et al. (1995) with their specific signal processing.
- The poorest performances are obtained at zero superficial liquid velocity: this should not be surprising since such flows do not exhibit strong unidirectional motion.
- Discarding stagnant conditions ($J_L = 0$ m/s), the relative error is maximum for gas fractions below 7%, i.e. in the finely dispersed regime. For R_{G3} above 7%, the error does not exceed −11%, with most results being about −5% or better. These findings are nearly the same as those reported by Zun et al. (1995) for similar gas fractions and their best expert. Yet, it should be mentioned that the relative error is slightly higher here, maybe due to the casing tubes which have an outer diameter of 3 mm, while Zun et al. used 0.9 mm outer diameter tubes.

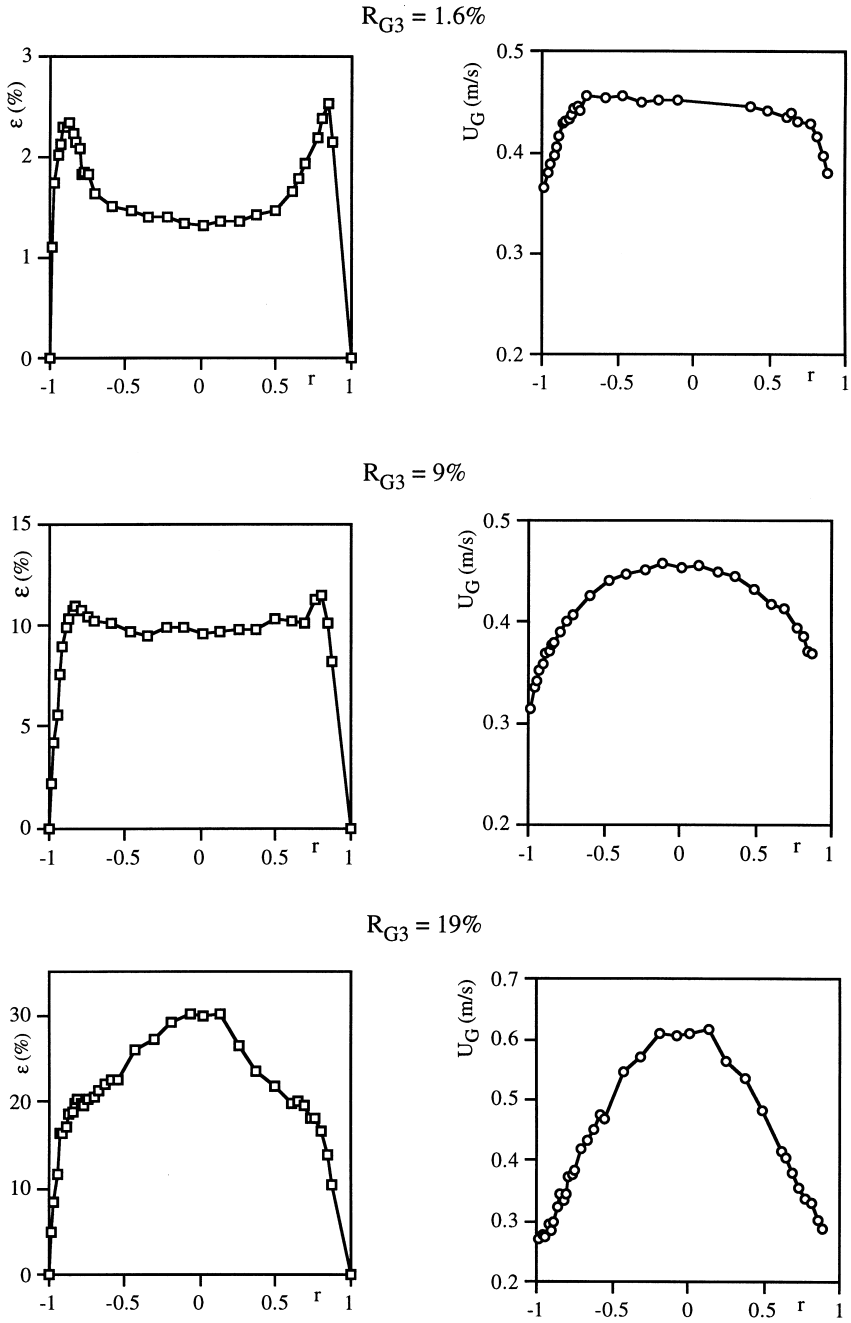

Fig. 13. Profiles obtained with a 3C probe at $J_L = 0.2$ m/s and various gas fractions (the probe enters the duct from $r = 1$).

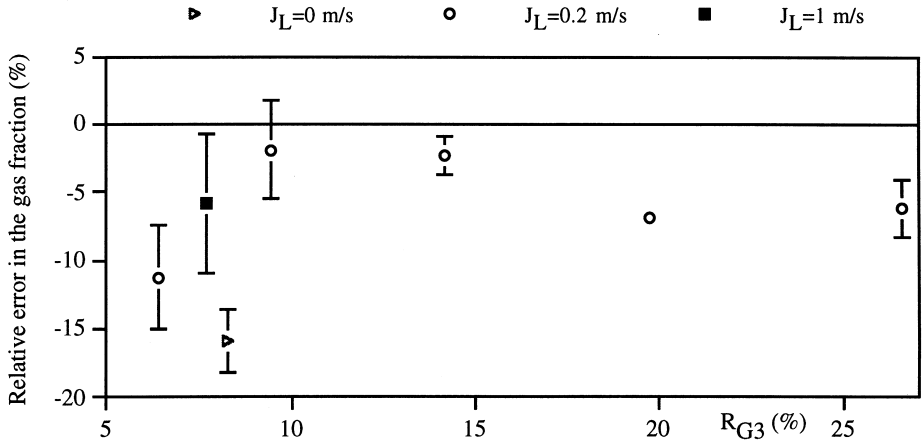

Fig. 14. Relative error in the gas fraction for a conical probe.

The fact that the void fraction is always underestimated, confirms the correct functioning of the real-time processing [underestimation was also the rule for Zun et al.'s results (Zun 1997 personal communication)]. Let us underline that, when absolute thresholding is calibrated against a reference technique, it sometimes occurs that some amount of noise must be interpreted as a gas phase in order to recover the expected void fraction. Such drawbacks being avoided here, the amount of error we have determined can be considered as a correct quantification of probe performance, almost free of bias effects due to the signal processing. It becomes then tempting to identify the parameters governing the phase-detection defects. From our limited set of data, no clear relationship can be perceived between the error and global quantities, such as the interfacial area density, the absolute velocity of the gas phase, or a typical bubble size. Such a breakdown is probably due to the variety of processes contributing

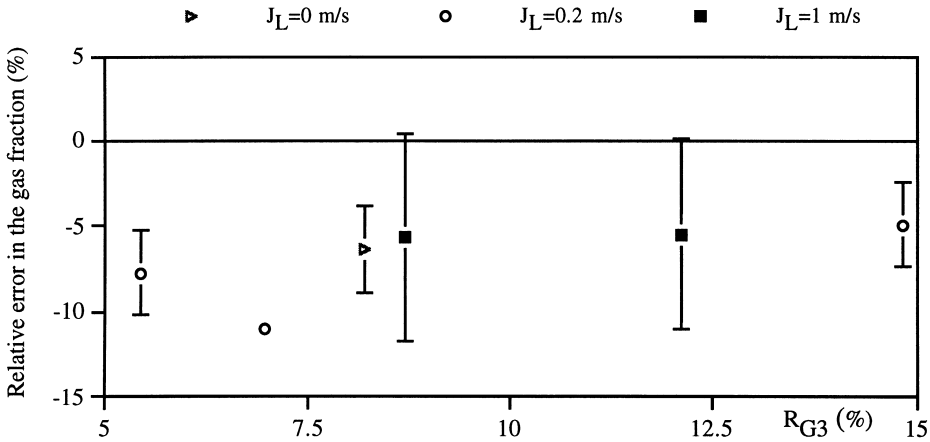

Fig. 15. Relative error in the gas fraction for a stretched monofiber probe.

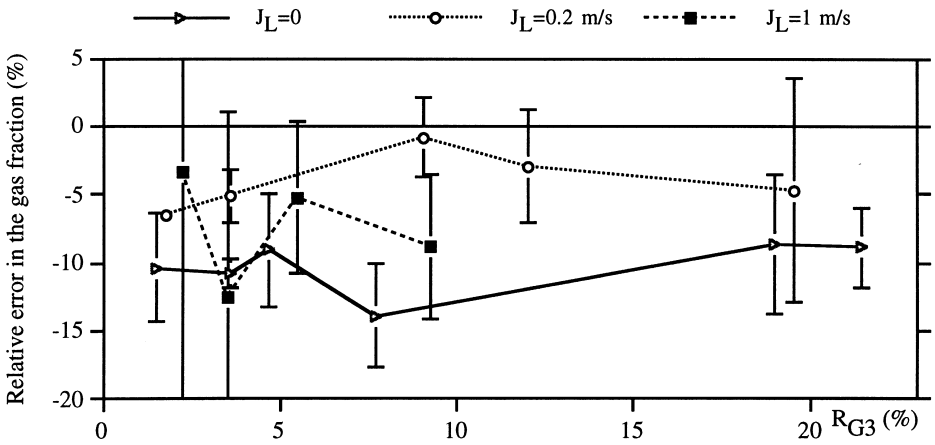

Fig. 16. Relative error in the gas fraction for a 3C monofiber probe.

to phase-detection error. Discarding processes such as splitting or sticking inclusions observed in liquid–liquid systems (see Sene 1984; Pinguet 1994) but less important in gas–liquid mixtures, three mechanisms remain:

1. The blinding effect: since the probe (at least those free of pre-signals) detects the disturbed interface position, the local interface deformation during probe impact contributes to the error. This leads to the definition of a "blind" zone or, equivalently, to an effective shape detected by a probe.
2. The drifting effect: the trajectory of the bubble is altered leading to either the detection of a smaller chord, or to no detection at all.
3. The crawling effect (a designation proposed by Serizawa et al. (1984) in their study of bubble–wire interaction): the whole bubble can be decelerated and/or deformed during the interaction.

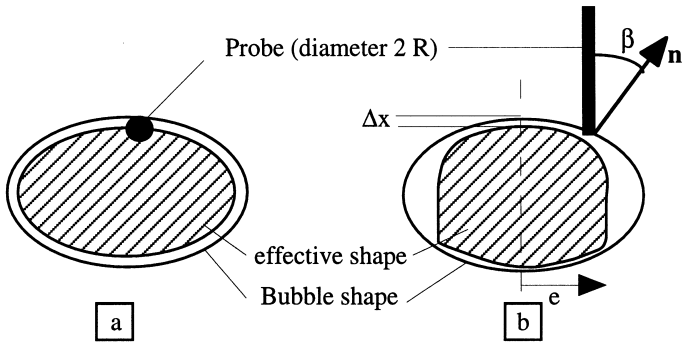

Fig. 17. Blinding effect and the effective bubble seen by a probe: (a) Carrica et al.'s model; and (b) probable behaviour.

The blinding and drifting effects are expected to be responsible for void fraction underestimation, while the crawling effect can have an opposite consequence as well.

For the first effect, Carrica et al. (1995) defined the blind zone as a membrane over the bubble interface of width equal to the probe tip radius ρ, Fig. 17(a). For convex bubbles randomly distributed in space and with the same direction of motion, their result rewritten for the relative void fraction error, and restricted to the first correcting term reads:

$$\text{relative error on } \varepsilon = -\frac{\Gamma}{\varepsilon}\rho \approx -6\frac{\rho}{D_{32}}, \tag{4}$$

where Γ is the mean interfacial area density and D_{32} the Sauter mean diameter of bubbles (contrary to the proposal of the authors and in agreement with the behaviour of our homemade optical probes, a minus sign has been maintained in (4)). Hence, for a given probe, i.e. for a fixed value of ρ, (4) predicts a strong decrease in the error as bubble size increases. No such trend has been observed in our experiments, although D_{32} varied by more than a factor of 5.

The blind zone being expected to be a strong function of the impact angle, a more realistic effective bubble shape can be introduced, Fig. 17(b). For moderate incidences β, the distortion arises mainly from the surge effect, i.e. the elevation Δx of the interface due to the inertia of the liquid phase occurring when the probe enters a bubble (the error during water entry is negligible at low velocities). Since probes are sensitive to the distorted interface location, they miss a portion of the gas dwell time proportional to Δx. Using a potential approximation, Δx has been evaluated for probes with a 30° cone angle travelling normal to a plane interface (Machane 1997). Denoting R the outer radius of the optical fiber, simulations provide the following fit:

$$\Delta x/R \approx 0.05\,(U_{\mathrm{i}}/U_0);\;\; U_0 := (g\,\sigma/\rho_{\mathrm{L}})^{1/4}. \tag{5}$$

For water–air systems, U_0 is about 0.16 m/s. Assuming (incorrectly) that (5) is valid for all impact angles, the relative underestimation on the void fraction equals $\Delta x/\langle \mathrm{C}\rangle$ where $\langle \mathrm{C}\rangle$ is the mean bubble chord. For a mean bubble size of 2 mm and a 140 μm outer diameter fiber, the relative error on the gas fraction would be about 3% at 1 m/s and 0.5% at 0.2 m/s. Hence, even if such a defect is not negligible at high velocities, it cannot account for our observations at moderate flow-rates.

For large impact angles, the de-wetting of the probe could not occur or could remain incomplete, so that the corresponding chords are either not perceived or underestimated, as sketched in Fig. 17(b). Former experiments with spherical bubbles have shown that no signal is detected by the probe above a critical eccentricity e_{c}, where e_{c} is typically 0.7 times the bubble radius for a 20 cSt fluid (Cartellier 1992—in these experiments, the blinding and drifting effects were not distinguished). Assuming that all chords corresponding to an eccentricity higher than e_{c} are ignored, the magnitude of the relative error on the void fraction is found to be:

$$\text{relative error on } \varepsilon = -\left[1 + \frac{\hat{e}_{\mathrm{c}}}{2}\left(\hat{e}_{\mathrm{c}}^2 - 3\right)\right], \tag{6}$$

where $\hat{e}_c = 2e_c/d$, and d is the bubble radius. (6) holds also for ellipsoidal bubbles provided that the eccentricity is scaled by half the long axis length. According to (6) a critical eccentricity of 0.7 (respectively, 0.8) corresponds to a relative error of about −12% (respectively, −6%). These magnitudes are in reasonable agreement with the observations of Figs. 14–16. However, e_c is expected to be sensitive to the liquid viscosity. According to Sene (1984), who has performed some experiments for a 200 μm outer diameter optical probe grounded to a 90° cone at its tip, all eccentricities are successfully scanned on bubbles in water of at least 3 mm in size and at absolute velocities higher than 30 cm/s. This result implies that no drifting occurs (an observation indeed reported by Sene). Such a behaviour would invalidate the blinding effect as a possible cause of incorrect phase detection in our experiments. However, in contradiction with Sene's results, we did observe drifting for 3 mm bubbles at 55 cm/s in water. Additional experiments are thus required to determine e_c in water, and it is presently quite difficult to appreciate the magnitude of phase detection defects associated with blinding and drifting.

To quantify the crawling effect, the data obtained during the qualification of a 140 μm outer diameter optical probe with a 30° cone at the extremity have been reexamined (Cartellier and Barrau 1998a). For single bubbles in water (long axis about 2 mm, short axis about 1.4 mm), the relative error in the chord intercepted by the conical probe has been measured, as well as the bubble deceleration. All bubbles were pierced along their axis of symmetry. The corresponding data, plotted in Fig. 18, show that the chord detected by the probe equals its actual value within ±10%. Since such a magnitude holds regardless of the deceleration experienced by the bubble, it seems that there is a sort of compensation between bubble deceleration and deformation. Similar trends have been observed by Sene (1984), who has also analysed the importance of the impact angle on the chord measurements. He concluded that, when averaging over all eccentricities, the chords detected were 10% smaller than actual values

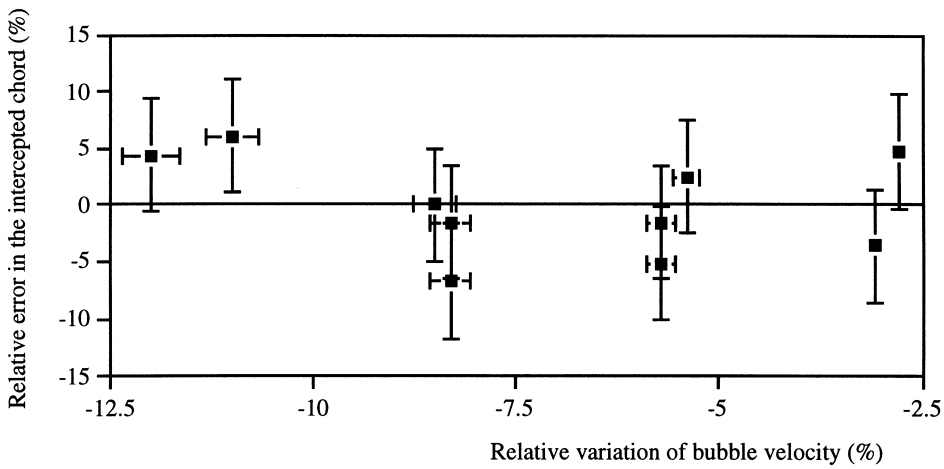

Fig. 18. Evolution of the relative error in the chord detected by a conical probe with the bubble deceleration (bubble in water, bubble velocity 55 cm/s).

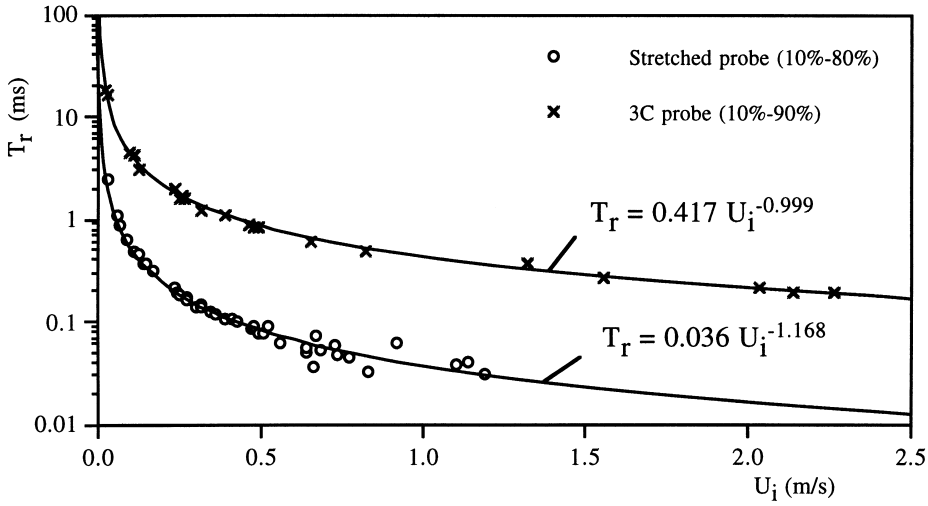

Fig. 19. Calibration of the $T_r(U_i)$ relationship for the stretched probe and the 3C probe.

for bubbles of a few millimetres in water. Therefore, the crawling effect appears also a plausible cause of incorrect phase detection.

The above magnitudes demonstrate that the two main origins of phase-detection uncertainties, i.e. the blinding and drifting effects on one hand and the crawling effect on another hand, are both likely to explain the observed discrepancies, and that there is not yet any indication of which is the dominant effect if any. Under such conditions, it is not surprising that our attempts to correlate the uncertainty to global parameters failed. Another consequence is that optical probe performance is difficult to predict if flow conditions are changed.

5.2. Error in gas flow-rate measurements

Let us turn now toward the qualifications on the gas flow-rate. To calibrate monofiber probes, the correlation between the rise time and the interface velocity were obtained under normal impacts in the facilities described in Cartellier 1992. The results are presented in Fig. 19 with the corresponding power law fits. Typically, the latency length, defined as the product of the interface velocity by the rise time, is about 36 μm for the stretched probe, while it is about 400 μm for the 3C sensor.

The relative deviation in the gas flow-rate obtained with the stretched monofiber probe is plotted in Fig. 20. The gas flow-rate is always underestimated by an amount not greater than 13%: since these deficits are close to those observed on the void fraction alone, it can be concluded that the gas velocity is well estimated. For the 3C probe in bubbly flows (Fig. 21), the gas flow-rate is recovered within $\pm 10\%$, except at very low gas fractions. For R_{G3} above 7%, errors in gas flow-rate and gas fractions have the same magnitude, indicating that the gas velocity is correctly determined. As the gas fraction decreases, the error in the gas flow-rate diminishes and becomes positive, indicating that the gas velocity is less accurate under these

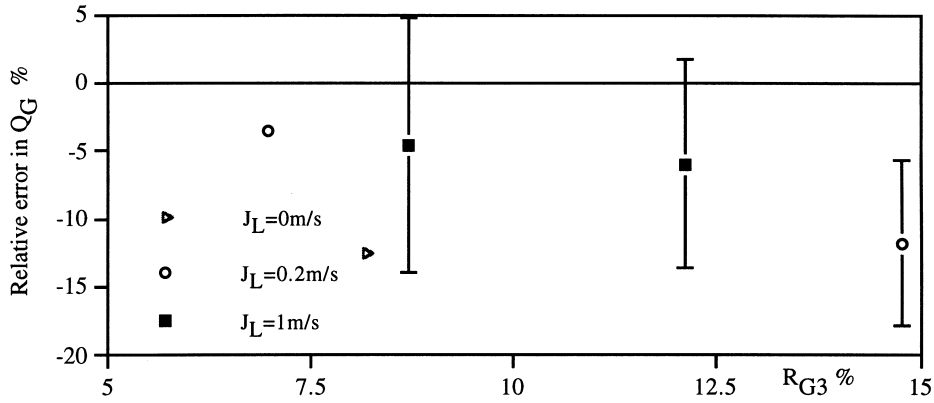

Fig. 20. Relative error in the gas flow-rate for a stretched monofiber probe.

conditions. The situation deteriorates at R_{G3} less than about 2%: the overestimation in the gas flow-rate is 16% for $J_L = 0.2$ m/s. It reaches 35% for stagnant conditions, probably because of the complex flow structure which generates odd bubble/probe interactions. It must be also noted that, as shown by Fig. 22, the largest errors in the gas flow-rate correspond to a low percentage of bubble signatures validated for velocity measurements (less than 45–50%), probably because the interpolation procedure required to estimate the gas flow-rate becomes more questionable under these conditions (See Section 2.2). Globally, the trends reported here are comparable with those obtained by Pinguet (1994) in dispersed oil/water flows with RF probes adapted to inclusion velocity measurements. This author obtained uncertainties in the oil flow-rate in the range ±20%, except at low dispersed phase fraction, where the oil flow-rate was strongly overestimated (about 70%).

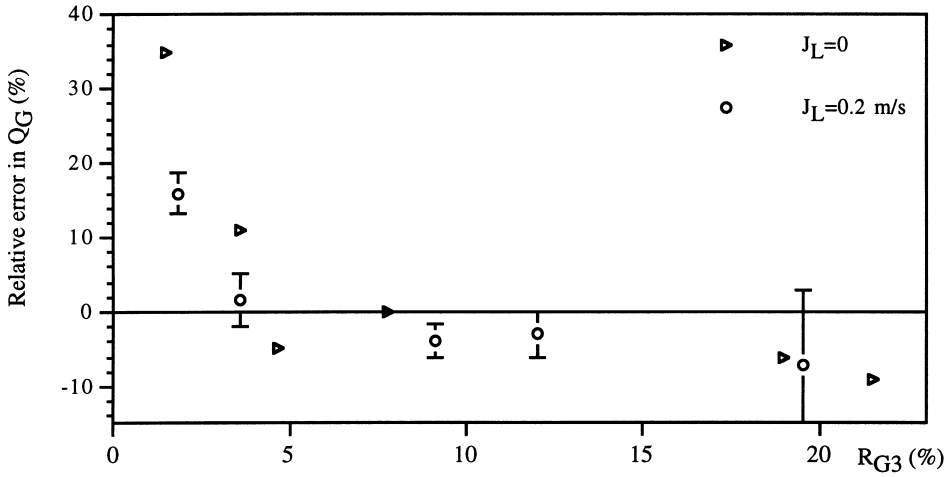

Fig. 21. Relative error in the gas flow-rate for a 3C monofiber probe in dispersed bubbly flows.

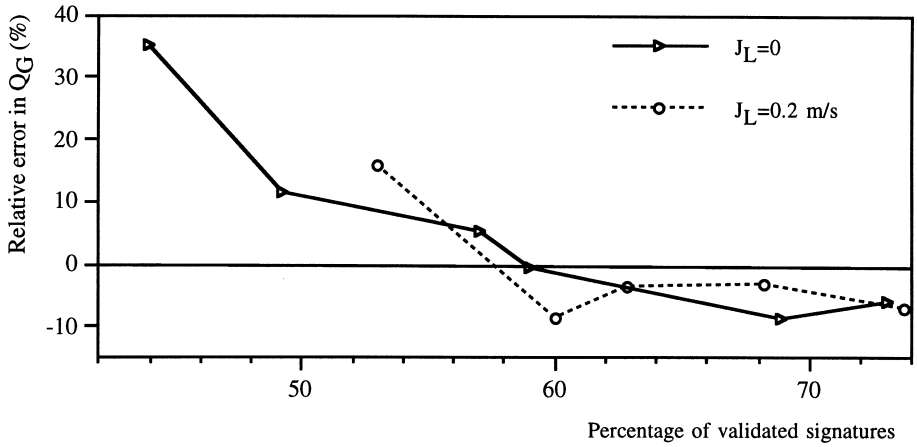

Fig. 22. Connection between the relative error in the gas flow-rate and the percentage of signatures validated for velocity measurements (case of a 3C monofiber probe in dispersed bubbly flows).

The performance of the 3C probe in transition and slug flows is given in Fig. 23. The gas flow-rate is strongly underestimated, while Taylor bubbles larger than 2 cm in size are present. This defect is not due to the percentage of validation, which is higher than 60% for all the data of Fig. 23. Instead, it is induced by our selection criteria which, as mentioned in Section 2.1, are not adapted to such bubble shapes. Since actual rise times at large impact angles are higher than expected from the $T_r(U)$ relationship (Cartellier and Barrau 1998b), velocities are indeed underestimated. As shown by the data of Fig. 21 for R_{G3} about 20%, for which the maximum bubble size was about 1 cm, the above selection problem does not occur for large wobbling bubbles, because the impact angle in this case scarcely takes important values. Hence, the limitation of our selection criteria is linked with the bubble shape more than with its size. The data in the right-hand side of Fig. 23 corresponds to a 10% overestimation of the gas

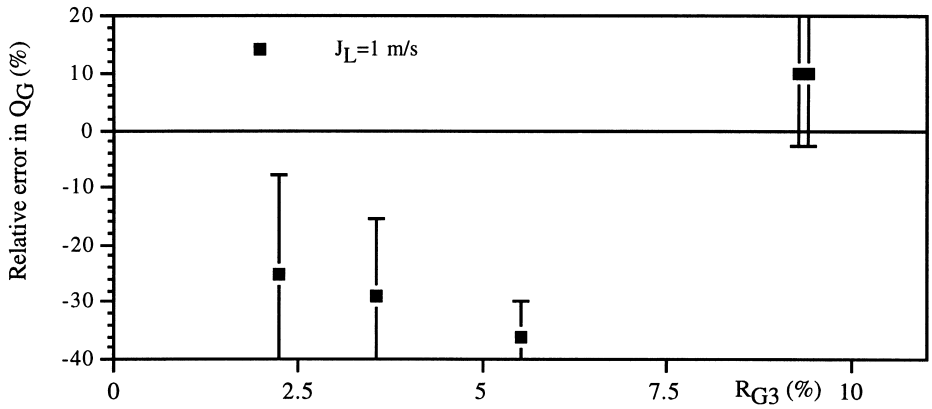

Fig. 23. Relative error in the gas flow-rate for a 3C monofiber probe in transition and slug flows.

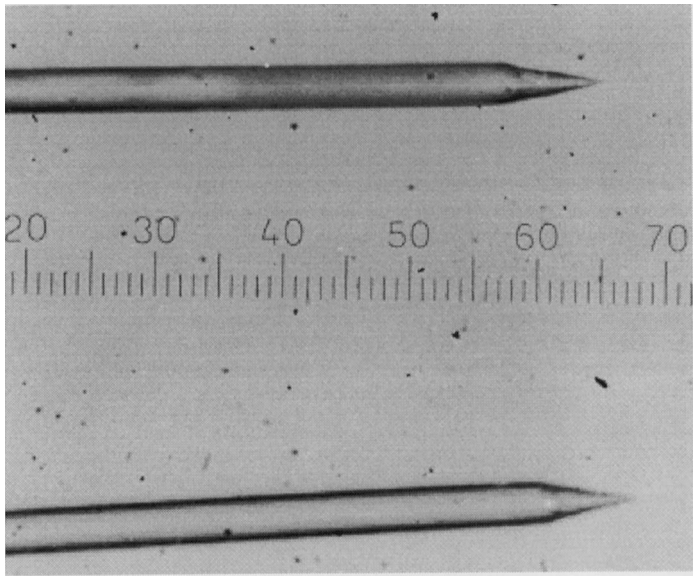

Fig. 24. Double-probe used during the qualification.

flow-rate in the slug regime. Another phenomenon comes here into play: due to the length of slugs, some liquid flows downward along the vertical holding tube and wets the probe tip before the rear of the slug impacts the sensor. This phenomenon, first noticed by Leblond (1995, private communication), is responsible for numerous distorted transients, for which the T_r (U) law is not valid. Again, the present selection criteria are unable to eliminate such events. Nevertheless, the gas flow-rate is obtained with reasonable confidence, but due to the limited flow conditions investigated, no definite conclusion can be drawn about the performance of 3C probes in slug flows.

Data has been obtained with a homemade double-probe composed of two conical probes with a tip–tip distance of 1.28 mm (Fig. 24). The results, given in Fig. 25 for an association

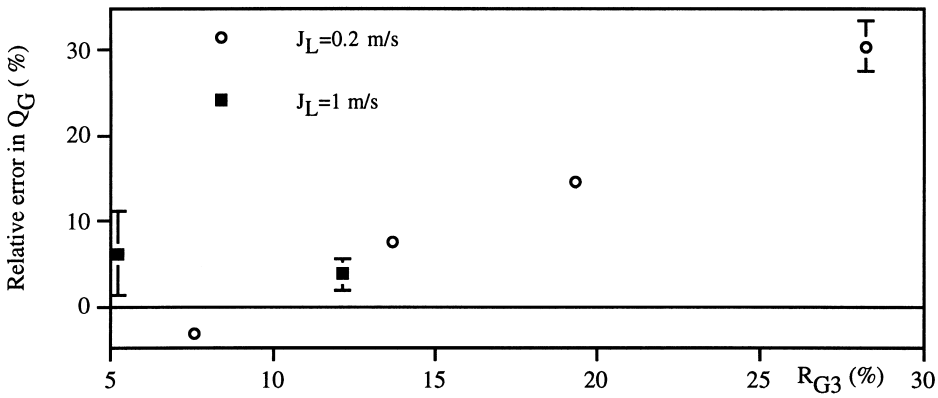

Fig. 25. Relative error in the gas flow-rate for a horizontal double-probe.

criterion of 5%, are almost the same up to $CSP = 10\%$. The gas flow-rate is nearly always overestimated. The error is less than 10% at moderate gas fractions, but increases steadily for R_{G3} higher than 20%. The latter behaviour is probably connected with the increase of incorrect pairing as more numerous interfaces impact the sensor, and as inclusion trajectories become more complex. According to the high level of the uncertainty (30%) obtained in a dense dispersed flow, the bi-probe technique can hardly be considered as a reference tool. However, bi-probes are better suited than the mono-probe technique for flows including Taylor bubbles, while the later technique is more efficient in dispersed two-phase flows.

6. Conclusion

A real-time processing for gas detection and gas velocity measurements using either mono- or bi-probes has been described. From knowledge of liquid and noise signal levels, it gives access to the entry and exit dates of all bubbles, and for some selected events to the rise time from which the inclusion velocity can be deduced. The good reliability of the signal processing has allowed evaluation of the true performances of various optical probes. The probe qualifications, achieved through a comparison between area- and volume-averaged gas fractions, have shown that the void fraction is within $+0/-16\%$ of its reference value, for the flow conditions and probes considered. If stagnant conditions are discarded, the average discrepancy drops to -6%. It has been shown that two mechanisms, namely the blinding–drifting effect and the crawling effect, provide equally plausible explanations for these defects. A more detailed analysis of bubble–probe interactions is, therefore, required before any significant scaling law could be proposed to estimate a priori the void measurement uncertainty. Accordingly, the magnitudes obtained in this paper cannot be considered as valid for flow conditions too different from those investigated. Notably, uncertainties are expected to increase in viscous fluids or in mixtures composed of tiny bubbles. Also, and as indicated by the results obtained for stagnant conditions, larger errors would occur in two-phase flows with strong three-dimensional and unsteady structures.

Inclusion velocity measurements with the monofiber technique have proven fairly accurate in dispersed bubbly flows even at high gas content. This technique, used either with stretched probes or with the new 3C probes, is more reliable than the bi-probe technique. However, it still requires refined selection criteria to properly analyse the signatures of hemispherical cap bubbles, so that bi-probes are recommended whenever such shapes are present.

Acknowledgements

The authors are grateful to the DER-EdF for support of this research under grant no. EdFT34L01/2K6727/RNE402.

References

Carrica, P., Sanz, D., Delgadino, G., Zanette, D., Di, Marco P., 1995. A contribution to uncertainties estimation of local void fraction measurements in gas–liquid flows. In: G. Celata, R. Shah (Eds.). Two-Phase Flow Modelling and Experimentation. Edizioni ETS, pp. 709–714.

Cartellier, A., 1990. Optical probes for local void fraction measurements: characterisation of performance. Rev. Sci. Instrum. 61 (2), 874–886.

Cartellier, A., 1992. Simultaneous void fraction measurement, bubble velocity, and size estimate using a single optical probe in gas–liquid two-phase flows. Rev. Sci. Instrum. 63 (11), 5442–5453.

Cartellier, A., 1999. Post-treatment for phase detection probes in non uniform two-phase flows. Int. J. Multiphase Flow 25 (2), 201–228.

Cartellier, A., Achard, J.L., 1991. Local phase detection probes in fluid/fluid two-phase flows. Rev. Sci. Instrum. 62 (2), 279–303.

Cartellier, A., Barrau, E., 1998a. Monofiber optical probes for gas detection and gas velocity measurements: conical probes. Int. J. Multiphase Flow 24 (8), 1265–1294.

Cartellier, A., Barrau, E., 1998b. Monofiber optical probes for gas detection and gas velocity measurements: optimised sensing tips. Int. J. Multiphase Flow 24 (8), 1295–1315.

Cartellier, A., Barrau, E., Poupot, Ch, Chambérod, E., 1996. Sondes optiques: innovations sur un capteur classique. La Houille Blanche 1/2, 120–128.

Clift, R., Grace, J., Weber, M., 1978. Bubbles, Drops and Particles. Academic Press, New York.

Fauquet, Ph, 1995. Mesure par monosonde optique en R12 en ébullition. Rapport TTA-DER-EdF HT-34/95/018/A, Chatou.

Garnier, J., 1997. Measurement of local flow pattern in boiling R12 simulating PWR conditions with multiple optical probes. In: Proc. OECD/CSNI Specialist Meeting on Advanced Instrumentation and Measurement Techniques, March 17–20, Santa Barbara, CA.

Grossetête, C., 1995. Experimental investigation and preliminary numerical simulations of void profile development in a vertical cylindrical pipe. In: A. Serizawa, T. Fukano, J. Bataille (Eds.). Proc. 2nd ICMF, April 3–7, Kyoto, Vol. 2, pp. IF1–1–10.

Hibiki, T., Hogsett, A., Ishii, M., 1997. Local measurement of interfacial area, interfacial velocity and liquid turbulence in two-phase flow. In: Proc. OECD/CSNI Specialist Meeting on Advanced Instrumentation and Measurement Techniques, March 17–20, Santa Barbara, CA.

Kataoka, I., Ishii, M., Serizawa, A., 1994. Sensitivity and analysis of bubble size and probe geometry on the measurements of interfacial area concentration in gas–liquid two-phase flow. Nucl. Engng Design 146, 53–70.

Kozma, R., 1995. Studies of the relationship between the statistics of void fraction fluctuations and the parameters of two-phase flows. Int. J. Multiphase Flow 21 (2), 241–251.

Leung, W., Revankar, S., Ishii, Y., Ishii, M., 1995. Axial development of interfacial area and void concentration profiles measured by double-sensor probe method. Int. J. Heat Mass Transfer 38 (3), 445–453.

Liu, W., Clark, N., 1995. Relationships between distributions of chord lengths and distributions of bubble sizes including their statistical parameters. Int. J. Multiphase Flow 21 (6), 1073–1095.

Machane, R., 1997. Contribution de la méthode intégrale aux frontières au suivi d'interface. Thèse, Institut National Polytechnique, Grenoble.

Miller, N., Mitchie, R., 1970. Measurement of local voidage in liquid/gas two phase flow systems using an universal probe. J. Brit. Nucl. Energy Soc. 2, 94–100.

Neal, L., Bankoff, S., 1963. A high resolution resistivity probe for determination of local properties in gas–liquid flow. AIChE J. July, pp. 490–494.

Pinguet, B., 1994. Étude de sondes d'impédance pour la caractérisation d'écoulements diphasiques liquide–liquide en conduite inclinée. Thèse, Univ. Pierre et Marie Curie, Paris.

Revankar, S., Ishii, M., 1992. Local interfacial area measurement in bubbly flow. Int. J. Heat Mass Transfer 35 (4), 913–925.

Revankar, S., Ishii, M., 1993. Theory and measurement of local interfacial area using a four sensor probe in two-phase flow. Int. J. Heat Mass Transfer 36 (12), 2997–3007.

Rossi, G., 1996. Error analysis based development of a bubble velocity measurement chain. Flow Meas. Instrum. 7 (1), 39–47.

Schmitt, A., Hoffmann, K., Loth, R., 1995. A transputer-based measuring system for decentralized signal processing applied to two-phase flow. Rev. Sci. Instrum. 66 (10), 5045–5049.

Sene, K., 1984. Aspects of bubbly two-phase flows. PhD., Univ. of Cambridge, UK.

Serizawa, A., Tsuda, K., Michiyoshi, I. 1984. Real-time measurement of two-phase flow turbulence using a dual-sensor anemometry. In: J.M. Delhaye, G. Cognet (Eds.). Measuring Techniques in Gas–Liquid Two-Phase Flows. Springer, New York. pp. 495–523.

Spindler, K., Hahne, E., 1995. Statistical analysis of void fraction for flow pattern identification in a natural and forced convection two-phase loop. In: G. Celata, R. Shah (Eds.). Two-Phase Flow Modelling and Experimentation 1995. Edizioni ETS, pp. 1339–1348.

Zun, I., Filipic, B., Perpar, M., Bombac, A., 1995. Phase discrimination in void fraction measurements via genetic algorithms. Rev. Sci. Instrum. 66 (10), 5055–5064.